Thermal Conductance of Ballistic Point Contacts

Th. Bartsch, M. Schmidt, Ch. Heyn, and W. Hansen

Institut für Angewandte Physik und Zentrum für Mikrostrukturforschung, Jungiusstraße 11, D-20355 Hamburg, Germany

(Received 30 September 2011; published 14 February 2012)

We study the thermal conductance of ballistic point contacts. These contacts are realized as few nanometer long pillars in so-called air-gap heterostructures (AGHs). The pillar length is orders of magnitude smaller than the mean free path of the phonons up to room temperature. Because of the small dimension and the low density of the pillars, the thermal conductance of the AGHs is several orders of magnitude reduced in comparison to bulk structures. The measurement results are in quantitative agreement with a simple model that is based on the Boltzmann transport equation.

DOI: 10.1103/PhysRevLett.108.075901 PACS numbers: 65.80.−g, 66.70.Df, 81.05.Ea, 85.80.Fi

Recent studies established significant influences on the thermal transport in solids by nanostructuring [1–3]. This opens the door for the realization of novel thermoelectric devices, where a low thermal conductance is essential [2–5]. In particular, using nanostructuring it is possible to scale the dimension of a solid to a regime where the mean free path (MFP) of the heat carrying phonons is larger than both the diameter and the length of the structure of interest [1]. The associated thermal-transport regime is named ballistic. So far there are many theoretical studies of ballistic thermal transport [6–9], which all emanate from the Boltzmann transport equation, but there are only few experimental data. Schwab *et al.* described experiments on suspended microstructures [1], but in those experiments the phonon MFP is larger than the dimension of the structure only at very low temperatures. Furthermore, a kind of ballistic thermal transport was observed in nanostructured systems such as superlattices [7], nanowires [8], and nanoparticles [10] where the phonon MFP is longer than the dimension of the nanostructure. However, interface and boundary scattering significantly influence the thermal transport in those structures and transmission coefficients are required to account for this [7–10]. In Ref. [11] we have demonstrated the fabrication of so-called air-gap heterostructures (AGHs) that enable the preparation of pillars with controlled length of a few nanometers. In the following, we demonstrate that these pillars represent pure ballistic thermal point contacts in a wide temperature range up to room temperature.

The AGHs are composed of a 50 nm GaAs capping layer that is supported by a number of nanopillars over a GaAs substrate. Here we investigate nanopillars with length of 4 and 6 nm, respectively. A schematic drawing of an AGH is shown in Fig. 1. The structures were fabricated using molecular beam epitaxy (MBE) with a combination of *in situ* local droplet etching [12–14] and *ex situ* selective chemical wet etching of a sacrificial layer. In the first MBE growth step an AlAs layer with thickness of 4 or 6 nm was deposited on a (001) GaAs substrate. This is followed by a Ga droplet etching step inside the MBE growth chamber, which generates in a self-organized fashion nanoholes deeper than the thickness of the AlAs layer [12–14]. These holes were filled by subsequent growth of a 50 nm thick GaAs layer. After removal of the sample from the MBE setup, a mesa was fabricated as described below. Finally, the AlAs layer was selectively removed by etching with a 5% solution of hydrofluoric acid, leaving the filled holes as GaAs nanopillars. Because of the MBE fabrication, the pillars are almost defect free and lattice matched to the substrate. A verification for this is given in Ref. [15] where transmission electron micrographs of similar heterostructures are discussed. We note that the capping layer keeps the perfect epitaxial relationship to the substrate crystal lattice, because the sacrificial AlAs and the GaAs have nearly the same lattice constant. A more detailed description of the preparation technique and a verification that the capping layers are separated from the substrate by the pillars was given in Ref. [11].

The thermal conductance was measured using the 3ω method. This method has been developed for measuring the thermal conductance of bulk materials and thin films [16–18]. A thin metal stripe on top of a specimen is used as heater and temperature sensor simultaneously. On our AGH samples we prepared a heater stripe with 1.6 mm length and 15 μm width by optical lithography and evaporation deposition of 30 nm Au. Afterwards, the semiconductor material aside from the heater was removed to a depth of 100 nm in a wet-etching step using the metal stripe as an etch mask. This prevents lateral heat spreading in the structure and opens the AlAs sacrificial layer for subsequent selective chemical wet etching.

For 3ω measurements, a sinusoidal ac current with frequency ω was driven through the heater. The generated

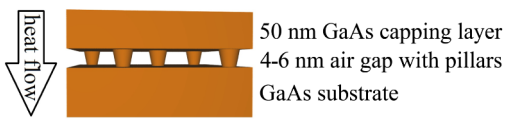

FIG. 1 (color online). Scheme of the investigated structure.

temperature oscillations induce a resistance oscillation at frequency 2ω. Thus the voltage drop across the heater includes a component at the frequency 3ω. Measurements of this 3ω voltage enable the determination of the temperature rise ΔT and finally of the thermal conductance of the material below the heater [16–18]. In the samples studied here, the AGHs are treated as a thin film between heater and substrate. Cahill *et al.* discussed such an experimental situation [17,18]. There it is assumed that the magnitude of the temperature rise ΔT is the sum of contributions from the film (ΔT_f) and the substrate (ΔT_s), if the film represents a significant thermal resistance R_f^{th} [17,18]:

$$\Delta T = \Delta T_f + \Delta T_s. \tag{1}$$

Below we describe how the contribution ΔT_f can be determined from the measured ΔT. Once ΔT_f is known, the thermal conductance K_f of the film can be calculated from the heating power P with the relation

$$\Delta T_f = R_f^{\text{th}} I_f^{\text{th}} = \frac{P}{K_f} \tag{2}$$

that is given by the general equation for a heat current I_f^{th} [17]. Note that the right side of the equation is only valid if the heat current through the film I_f^{th} is equal to the power P impressed by the heater; i.e., heat losses are neglected [17].

In previous publications, ΔT_f was determined with a differential technique by measuring one sample with the investigated film (ΔT) and a second reference sample with a heater directly on the substrate (ΔT_s) [17,18]. In our experimental approach we are able to execute both measurements on the same sample. The first measurement is performed before etching of the sacrificial AlAs layer and the second afterwards. The temperature rise on the unetched sample is expected to be equal to the temperature rise ΔT_s on a GaAs substrate, since the specific thermal resistance of the thin AlAs is nearly identical compared to the substrate. To verify this we performed measurements on the unetched sample and an intrinsic GaAs substrate, which exhibit no significant differences. In the next step, after determining ΔT_s on the unetched sample, we selectively etched the AlAs to uncover the pillars. Now the 3ω measurements were repeated to determine ΔT. Figure 2 shows exemplarily how the etching influences the temperature rise. As expected, ΔT is significantly larger after etching. We associate the difference ΔT_f to the higher thermal resistance of the AGHs after etching. The slopes of the temperature rises ΔT and ΔT_s are nearly equal. This is expected and indicates that the slopes are not affected by the presence of the film below the heater; i.e., the slope is just influenced by the substrate [17,18]. Using the relation between the slope and the thermal conductivity of the substrate established by Cahill in Ref. [16], we determined the thermal conductivity of the substrate. The results are in good agreement with the literature values for GaAs thermal conductivity [19,20]. This indicates that the 3ω method is applicable to the AGH samples studied here.

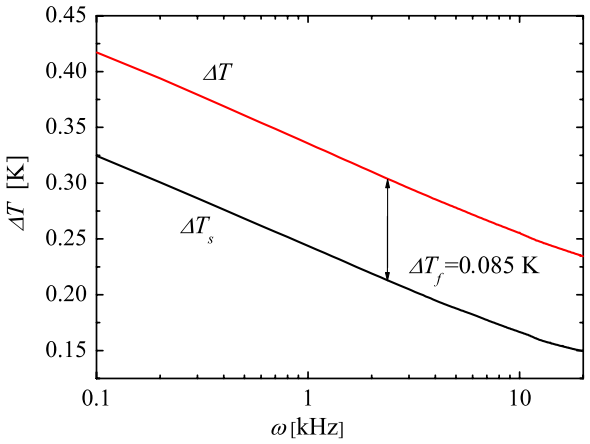

FIG. 2 (color online). Temperature rise as function of frequency determined from 3ω measurements at $T = 300$ K on an AGH sample with 6 nm long pillars. The black line represents the measurement before and the gray (red) line after selective removal of the AlAs layer.

We determined the thermal conductance of the pillar ensembles in the AGHs in the temperature range between 20 and 300 K with Eq. (2) from the measured 3ω data. The spreading of our data at comparable conditions is less than 15%, which is smaller than the error of 20% estimated by Borca-Tasciuc *et al.* [18] for 3ω measurements on thin films by using the differential technique with two samples. Figure 3 presents conductances of AGHs with 4 and 6 nm long pillars. An increase of the thermal conductance of the AGHs with increasing temperature is clearly visible. For temperatures higher than 150 K, the measured values

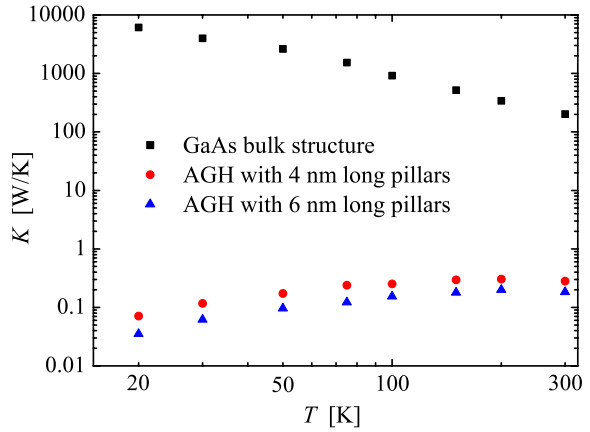

FIG. 3 (color online). Thermal conductance of two AGH samples and a GaAs bulk structure (black squares) calculated as reference as described in the text. The red points correspond to an AGH with 4 nm long pillars and the blue triangles to an AGH with 6 nm long pillars. The size of the symbols is equal to the error bars in the logarithmic plot.

saturate. On average the thermal conductance of the 4 nm AGH is 1.75 times higher than that of the 6 nm AGH. For comparison, we calculate the thermal conductance of GaAs bulk material with dimensions of the air gaps. For this purpose, we neglected any surface effects; i.e., we just multiplied the thermal conductivity of the substrate by the area of the heater and divided it by the average length of 5 nm. A comparison of the thermal conductance of AGHs and GaAs bulk is presented in Fig. 3. It shows firstly that the thermal conductance data of the AGHs are orders of magnitude smaller and secondly that the slope of the temperature dependence is inversed. We also calculated a bulk thermal conductance of a structure with the cross section of the pillars alone. From the pillar diameters and densities determined below we estimate that the pillars represent 3%–5% of the total AGH cross section. This would reduce the calculated bulk conductance by a factor of 20–35. Nevertheless, it is still up to 3 orders of magnitude larger than the measured thermal conductance of the AGHs in the temperature range studied. Note, however, that conductance values calculated from a diffusive model become treacherously large if the pillar length is smaller than the phonon MFP of the diffusive model. Obviously, the thermal conductance of the AGHs is determined by different mechanisms compared to the bulk material.

To explain the measured thermal conductances of the AGHs we assume a simple model, in which the thermal conductance is mainly determined by phonon transport through the pillars. At $T = 300$ K the bulk MFP of the phonons in GaAs is 145.3 nm [7]. Since the pillars are much shorter than the bulk MFP and they are also defect and interface free [15], we assume that the phonon current through the pillars is not influenced by phonon scattering but rather by the probability that a phonon passes through the pillars. This scenario is analogous to a current of gas molecules that passes through a hole in a containment or to ballistic electrons passing a Sharvin-point contact [21]. Thus, in our model each pillar represents a thermal point contact that connects two half-spaces with a phonon gas. In each half-space, the phonon gas is in equilibrium at a certain temperature. This assumption is reasonable because the thermal conductances of the capping layer and the substrate are orders of magnitude larger compared to the air gap. The ballistic heat current $I^{\mathrm{th}}_{\mathrm{pillar}}$ through a single pillar follows from the Boltzmann transport equation [7–10]

$$I^{\mathrm{th}}_{\mathrm{pillar}} = A \sum_{p=1}^{3} \int_{k=0}^{k_{\max}} \frac{1}{(2\pi)^3} [f(k, T_h) - f(k, T_c)] \hbar\omega_p(k) v_p(k) \cos(\theta) d^3k, \quad (3)$$

where A is the cross-sectional area of the pillar, k is the wave number of the phonons, $f(k, T)$ is the Bose-Einstein distribution at temperatures T_h and T_c of the hot and cold half space, respectively. The phonon energy is $\hbar\omega_p$ and $v_p \cos(\theta)$ is the phonon group velocity component in the direction of the heat current. The sum considers three phonon polarizations p, one longitudinal and two transversal acoustic phonon modes. The optical phonon modes are neglected because of their low velocities and high activation energies [7]. To simplify the integral in Eq. (3), we substitute $x_p = \hbar\omega_p / k_B T$ and approximate the dispersion relation for the fcc GaAs crystal in the (001) direction by

$$\omega_p(k) = \omega_p^{\max} \sin\left(\frac{ka}{4}\right), \quad (4)$$

with the lattice constant a and the maximum phonon frequency $\omega_p^{\max}$. The values of $\omega_p^{\max}$ are taken from Ref. [22]. Finally, dividing $I^{\mathrm{th}}_{\mathrm{pillar}}$ by the temperature difference of the phonon gases results in the thermal conductance of a single pillar:

$$K_{\mathrm{pillar}} = \frac{I^{\mathrm{th}}_{\mathrm{pillar}}}{\Delta T} = \frac{2}{\pi^2} \frac{k_B^2 T}{\hbar} \frac{A}{a^2} \sum_{p=1}^{3} \int_{x_p=0}^{x_p^{\max}} [\arcsin(x_p / x_p^{\max})]^2 \times \frac{x_p^2 e^{x_p}}{(e^{x_p} - 1)^2} dx_p. \quad (5)$$

To solve this equation the cross-sectional area A of the pillars is required. Moreover, since we measure the thermal conductance of an ensemble of pillars, the pillar density is needed to quantitatively compare the model results with the measurements.

Because of the fabrication method the structural parameters of the pillars are determined by the initial nanoholes. So far, measurements on AlAs surfaces are not available, which is due to the very fast oxidation of the highly reactive AlAs under air. Therefore, we estimate the structural parameters of the pillars from atomic force microscopy of nanoholes created by local droplet etching in $Al_{0.35}Ga_{0.65}As$ and GaAs surfaces. In previous publications the total hole density was about 2 μm^{-2} [12] and the average diameter was 100 nm [13]. The atomic force microscopy data show in addition a broad hole depth distribution with a high density of holes with depth between 4 and 6 nm [14]. Those holes contribute to the density of the pillars in the 4 nm AGH sample but not to the 6 nm AGH. This qualitatively explains the different thermal conductances measured here for 4 and 6 nm AGH samples. While in perfect ballistic point contacts a pillar length independent conduction is expected, our raw data show slightly different conductions, which we attribute to the different densities of participating pillars as described above. Because of the uncertainties of the hole densities and depth distribution on AlAs, we consider the respective pillar densities in 4 and 6 nm AGH as fitting parameter, while we take the diameter fix on 100 nm, to compare the measurements with the model. We obtain best agreement using a density of 6.4 μm^{-2} for the 4 nm long and

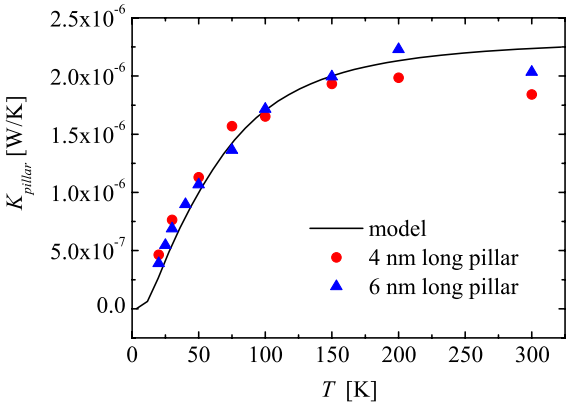

FIG. 4 (color online). Thermal conductance of a single pillar. The full line is calculated according to the model Eq. (5), assuming a pillar diameter of 100 nm. As described in the text, the points are calculated from the data in Fig. 3 assuming slightly different pillar densities for AGHs with 4 and 6 nm long pillars, respectively.

3.75 μm^{-2} for the 6 nm long pillars. The higher pillar densities determined here are probably related to a reduced coefficient for surface diffusion of Ga droplets on AlAs surfaces in comparison to $Al_{0.35}Ga_{0.65}As$ and GaAs surfaces and a thus increased hole density. The comparison of the experimental data and the model is shown in Fig. 4. Only at 300 K we find a considerable difference. This might be associated to the fact that at 300 K the phonon MFP becomes comparable to the pillar diameter. The very good agreement between model results and experimental data indicates that the thermal conductance of the AGHs is dominated by the proposed mechanism of ballistic heat transport through the pillars.

The key result that the insertion of an air gap with low density nanopillars reduces thermal conductance several orders of magnitude may pave the way to novel thermoelectric devices with large efficiencies [2–5]. Because of the adjustable small gap sizes and the epitaxial relationship between capping layer and substrate, the AGHs are probably useful for investigations of thermionic effects [4,5].

In conclusion, we have measured the thermal conductance of short GaAs nanopillars. The lengths of the pillars are well below the phonon MFP up to room temperature. A simple model of ballistic thermal transport through point contacts was introduced to explain the experimental results. The model exhibits very good qualitative agreement with the experimental conductance data. The agreement is also quantitatively good, if we assume pillar diameters and densities that are in the range of earlier measurements. This supports our approach of pure ballistic thermal transport in the pillars. Furthermore, the observed thermal conductances are orders of magnitude smaller than in comparable structures with specific thermal conductivity of GaAs bulk material. Based on this reduction, the AGHs may open the door for new thermoelectric devices with enhanced efficiencies [2–5]. Electrical transport studies through doped pillars are pending for thermopower studies.

This work was supported by the Deutsche Forschungsgemeinschaft via HA 2042/6-1, GrK 1286, and SSP 1386. Also we thank David Sonnenberg for helpful discussions and the growth of samples for the determination of the pillar structural parameters.

[1] K. Schwab, E. A. Henriksen, J. M. Worlock, and M. L. Roukes, Nature (London) **404**, 974 (2000).
[2] C. J. Vineis, A. Shakouri, A. Majumdar, and M. G. Kanatzidis, Adv. Mater. **22**, 3970 (2010), and references therein.
[3] A. Majumdar, Science **303**, 777 (2004).
[4] T. Zeng, Appl. Phys. Lett. **88**, 153104 (2006).
[5] T. L. Westover and T. S. Fisher, Phys. Rev. B **77**, 115426 (2008), and references therein.
[6] D. E. Angelescu, M. C. Cross, and M. L. Roukes, Superlattices Microstruct. **23**, 673 (1998).
[7] G. Chen, Phys. Rev. B **57**, 14958 (1998), and references therein.
[8] N. Mingo, Phys. Rev. B **68**, 113308 (2003).
[9] R. Prasher, Phys. Rev. B **74**, 165413 (2006).
[10] P. E. Hopkins, M. M. Mittal, L. M. Phinney, A. M. Grillet, and E. M. Furst, Appl. Phys. Lett. **99**, 133106 (2011).
[11] Ch. Heyn, M. Schmidt, S. Schwaiger, A. Stemmann, S. Mendach, and W. Hansen, Appl. Phys. Lett. **98**, 033105 (2011).
[12] Ch. Heyn, A. Stemmann, and W. Hansen, Appl. Phys. Lett. **95**, 173110 (2009).
[13] A. Stemmann, Ch. Heyn, T. Köppen, T. Kipp, and W. Hansen, Appl. Phys. Lett. **93**, 123108 (2008).
[14] Ch. Heyn, A. Stemmann, and W. Hansen, J. Cryst. Growth **311**, 1839 (2009).
[15] A. Nemcsics, Ch. Heyn, L. Toth, L. Dobos, A. Stemmann, and W. Hansen, J. Cryst. Growth **335**, 58 (2011).
[16] D. G. Cahill, Rev. Sci. Instrum. **61**, 802 (1990).
[17] D. G. Cahill, M. Katiyar, and J. R. Abelson, Phys. Rev. B **50**, 6077 (1994).
[18] T. Borca-Tasciuc, A. R. Kumar, and G. Chen, Rev. Sci. Instrum. **72**, 2139 (2001).
[19] R. O. Carlson, G. Slack, and S. Silverman, J. Appl. Phys. **36**, 505 (1965).
[20] P. D. Maycock, Solid State Electron. **10**, 161 (1967).
[21] Y. V. Sharvin, J. Exp. Theor. Phys. **48**, 984 (1965).
[22] J. S. Blackemore, J. Appl. Phys. **53**, R123 (1982).